ACS OMEGA

http://pubs.acs.org/journal/acsodf

Article

Preparation and Properties of Organic–Inorganic Hybrid Antireflection Films Made by a Low-Temperature Process Using Hollow Silica Nanoparticles

Ryo Muraguchi,* Wataru Futagami, Yuko Hakoshima, Keisuke Awaya, and Shintaro Ida*

Cite This: *ACS Omega* 2021, 6, 8570–8577

Read Online

ACCESS | Metrics & More | Article Recommendations | Supporting Information

ABSTRACT: Layers made of hollow silica nanoparticles have potential applications as antireflection films with lower refractive index values compared with existing materials such as silica glass (1.50) and magnesium fluoride (1.38). The advantages of such nanoparticles result from interactions between the solid shell, the cavity phase core, and the voids between particles. To obtain practical antireflection films, it is necessary to control the number of layers of these hollow silica nanoparticles and to fill the gaps between particles with a solid. In the present study, antireflection films were prepared by applying a coating of hollow silica nanoparticles dispersed in a UV-curable monomer solution onto plastic substrates. After film formation and exposure to UV light, the voids between the nanoparticles were completely filled with a polymer matrix. Tuning the particle concentration in the coating solution allowed the formation of antireflection films comprising one to three layers of the hollow silica nanoparticles. The reflectance of the films was dependent on the number of layers, and a 100 nm thick film in which two layers of hollow silica nanoparticles were precisely arranged showed the lowest reflectance of 0.92% at 550 nm wavelength, equivalent to a refractive index of 1.23. Because the voids between particles were filled with the polymer, these films resisted contamination during manual handling and so would be expected to maintain low reflectance during practical applications. This work demonstrates that nanosized inorganic–organic hybrid films composed of hollow silica nanoparticles and a UV-curable resin can exhibit optical properties and structural integrity that cannot be achieved by either substance alone.

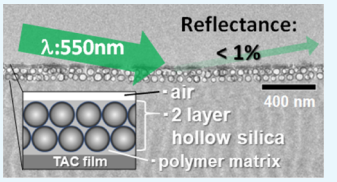

INTRODUCTION

Hollow nanoparticles have attracted much attention in various fields,[1−7] with potential applications in catalysis and drug delivery as well as in anticorrosion, antireflection, and superhydrophobic coatings.[8−10] These materials are typically synthesized using template methods and have pores from 20 to 50 nm in size in their core regions, with solid shells having thicknesses in the range of 10−50 nm. Films composed of these hollow nanoparticles have exhibited various optical, electrical, and thermal properties that differ from those of the shell materials as bulk solids. This occurs because the characteristics of the nanoparticles are determined by the effects of both the core and shell parts as well as the gaps between particles.

Antireflection coatings can be obtained by applying a single-layer coating of a material with a refractive index of 1.22 to a glass surface with a refractive index of 1.5. However, magnesium fluoride (MgF_2), which is widely used as a material having a low refractive index,[11,12] has a refractive index of 1.38 and so still generates 1.4% reflection. It would thus be desirable to develop thin films with lower refractive index values that can be easily formed and that provide antireflection properties over relatively wide ranges of wavelength and incident angles as single layers. Thus, a current challenge in the study of reflection reduction technology is the fabrication of low refractive index surface layers. There are currently no materials with low refractive index values on the order of 1.1 or 1.2. Therefore, it will be necessary to fabricate structures smaller than the wavelengths of light impinging on the glass surface to effectively lower the refractive index. Possible approaches to producing low refractive index films include employing a porous, sponge-like microstructure or generating a distribution of refractive index values based on a microprojection structure. The principles associated with these reflection reduction techniques are well known and have been researched for some time now. In recent years, new developments have been made since the appropriate technology for controlling and forming surface microstructures, including material technology, has been established. So far, thin-film materials with a refractive index of 1.1−1.2 have been reported, such as a porous film[13] using SiO_2 nanorods and a composite film[14] of hollow silica particles and alkoxide hydrolyzate; however, there are no hollow silica-film-filled gaps between particles with the polymer in a low-temperature process below 100 °C.

Received: January 21, 2021
Accepted: March 4, 2021
Published: March 16, 2021

https://doi.org/10.1021/acsomega.1c00386
ACS Omega 2021, 6, 8570–8577

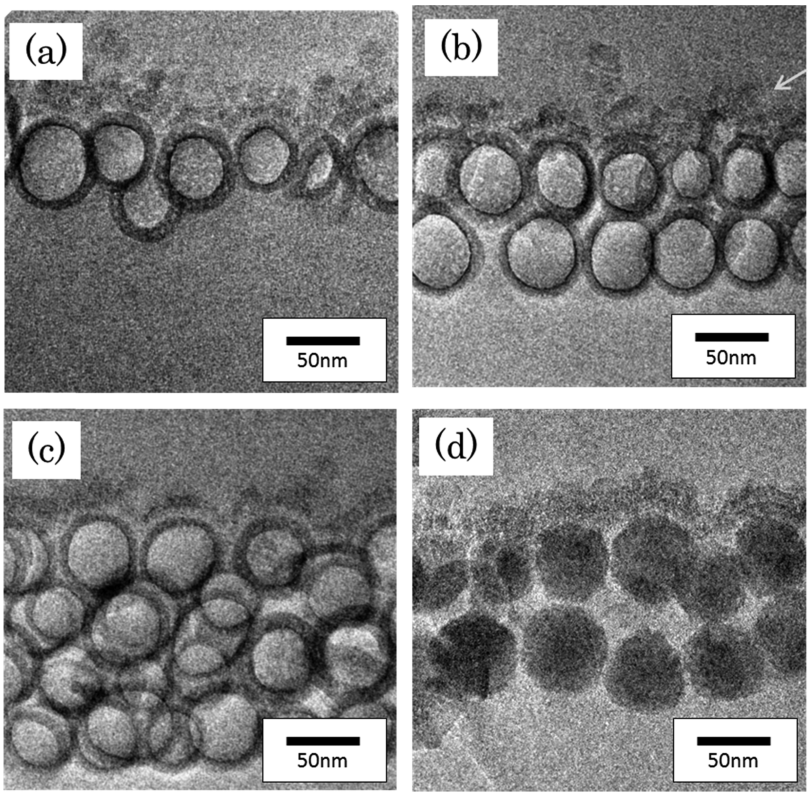

Figure 1. Cross-sectional TEM images of the (a) 1-layer-h-SiO_2, (b) 2-layer-h-SiO_2, (c) 3-layer-h-SiO_2, and (d) 2-layer-d-SiO_2 antireflection films. The arrow in figure (b) indicates the oil black ink painted on the surface.

Hollow silica nanoparticles are one of the most promising materials for antireflection coatings[15−20] because they are chemically stable, corrosion and heat resistant, and exhibit significant hardness. In addition, films composed of these nanoparticles have shown lower refractive index values than silica itself (n = 1.46),[21] meaning that they have antireflection properties. Such antireflection coatings[22,23] can both suppress the reflection of light from a substrate and improve light transmittance.[24−27] Consequently, antireflection and low-reflection coatings can increase the power generation efficiency of photovoltaic panels and the visibility of television and mobile device displays. In fact, with recent improvements in display resolution, the development of antireflection coating with reflectances of less than 1% is now required. In the case of mobile displays, ultrathin film substrates composed of polymers such as polyethylene terephthalate (PET) or triacetyl cellulose (TAC) are typically used. These materials are heat resistant up to approximately 100 °C, and so it is highly desirable to be able to process antireflection coatings below this temperature. In addition, mobile display surfaces are designed to be frequently touched by hand, and therefore, it is necessary for these surfaces to resist the penetration of sebum and other naturally occurring substances into the voids between hollow silica nanoparticles. Normally, substances such as sebum will readily penetrate into the gaps between nanoparticles because these regions are simply filled with air. It is difficult to remove these contaminants, which reduce visibility and increase reflectivity.

To meet these challenges, it is necessary to apply hollow silica nanoparticles with uniform sizes and pores onto a substrate while controlling the nanolevel thickness (100 nm) and maintaining a high density of the particles, operating below 100 °C. In addition, the gaps between the nanoparticles should be filled with a material such as a polymeric matrix. However, these aspects of film processing have been difficult to achieve to date. Jia et al.[28] fabricated a 250 nm thick gradient refractive index coating on a glass substrate and obtained 99.04% transmittance but required high-temperature thermal treatment at 550 °C. Ye et al.[29] reported a method for film formation on a glass substrate below 100 °C using hollow silica nanoparticles prepared in advance. Cohen et al.[30] described a method for film formation on a poly(methyl methacrylate) (PMMA) substrate below 100 °C using layer-by-layer assembly. However, the gaps between the nanoparticles were not filled with a polymeric matrix.

In the present work, we prepared antireflection thin films on TAC substrates using a bar coating technique, in conjunction with a mixture of hollow silica nanoparticles (diameter: 60 nm, shell thickness: 8 nm) and a UV-curable acrylate monomer. As a result, an antireflection film with a reflection of less than 1% was successfully prepared below 100 °C. This film comprised two layers of hollow silica nanoparticles with the gaps between the nanoparticles filled with the polymer. The nanoparticles were precisely arranged on the substrate at a high density. The film showed low haze and high transparency values as a result of the lack of voids between the nanoparticles.

RESULTS AND DISCUSSION

Figure 1 presents cross-sectional transmission electron microscopy (TEM) images of the antireflection coating films produced using the AR-1-AR-4 paints. The blending ratios of coating paints (AR-1-AR-4) are shown in Table 1. In the case of the AR-1 film, the hollow silica nanoparticles were aligned in a single particle layer at the top of the film (Figure 1a). The

https://doi.org/10.1021/acsomega.1c00386
ACS Omega 2021, 6, 8570−8577

Table 1. Parameters Used to Prepare Liquid Antireflection Coatings

	hollow silica sol [g]	dense silica sol [g]	IPA [g]	MIBK [g]	PETA [g]	HCPK [g]
AR-1	0.33		6.59	2.75	0.23	0.11
AR-2	0.66		6.63	2.49	0.15	0.08
AR-3	0.92		6.66	2.29	0.09	0.05
AR-4		0.48	6.65	2.71	0.11	0.05

TEM observations confirmed that these nanoparticles were uniformly arranged even when contained in the UV-curable organic resin, without any apparent aggregation. The average diameter of the nanoparticles was approximately 60 nm and each nanoparticle had a shell layer (shown as a dark contrast in the TEM images) with a thickness of about 8 to 10 nm. Hereafter, the antireflection coating made from the AR-1 paint is abbreviated as the 1-layer-h-SiO_2 film. Figure 1b shows a cross-sectional TEM image of an antireflective coating film made from the AR-2 paint. In this specimen, the hollow silica nanoparticles were arranged in a two-layer structure within the film, and the particles in the upper and lower layers were in a zigzag pattern similar to a close-packed structure. In general, dispersions of colloidal nanoparticles exhibit strong interactions between the nanoparticles due to their large surface areas, such that these nanoparticles are often aggregated during the film formation or drying processes. However, Figure 1b demonstrates that such aggregation did not occur in the present work, and that the nanoparticles underwent self-assembly with good packing. As for the mechanism for avoiding agglomeration, the following two processes, as shown in Scheme 1, are important. One is the process to prevent the

Scheme 1. Preparation of UV-Curable Antireflection Coating Paint

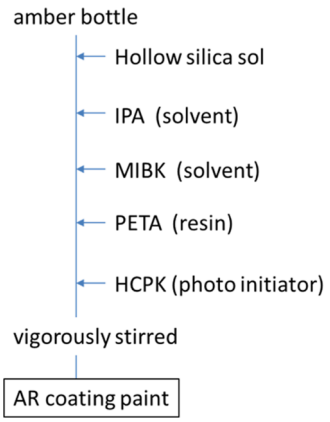

hollow silica nanoparticles from being directly mixed with acrylate resin (pentaerythritol triacrylate, PETA), and the other one is the process in which the concentration of hollow silica nanoparticles dispersion is diluted with a solvent (isopropyl alcohol, IPA and methyl isobutyl ketone, MIBK) as much as possible before being made into a paint. These two processes will be one of the factors that alleviate the dispersion shock of sol dispersion. In addition, choosing a solvent with highest solubility parameter possible and diluting in that order can also help prevent nanoparticles from aggregating. In addition, the cross-sectional view indicates that the gaps between the upper and lower particles were filled, such that no voids were present other than the internal spaces within the hollow particles. These gaps between nanoparticles were evidently filled by the polymerized PETA. Assuming that the 60 nm nanoparticles were densely packed in upper and lower stages, a film height of approximately 112 nm would be expected. In reality, the packing was not ideal because there was a distribution of nanoparticle sizes, but the cross-sectional view in Figure 1b shows that a film having approximately this theoretical morphology was formed. Regarding the penetration resistance of sebum, it was evaluated by painting the surface of the film with oil black ink. The black parts indicated by the arrow in Figure 1b correspond to the oil black ink. The penetration of the oil black ink into the film was not observed, indicating that the obtained film has a resistance to the penetration of organic compounds into the film. Note that black ink was applied to the film surfaces of the TEM samples so that these surfaces could be more easily identified. The cross-sectional view in Figure 1b also indicates that the upper part of the hollow silica nanoparticles in the upper layer (that is, the surface of the antireflection coating film) was covered with a polymeric coating rather than the particles being exposed. That is, although the film surface was somewhat rough due to the inclusion of the nanoparticles, these nanoparticles were embedded within the film and the gaps between them were filled with the resin such that there were no voids between particles. This sample is referred to as the 2-layer-h-SiO_2 film. Figure S1 shows the field-emission scanning electron microscopy (FE-SEM) image of the 2-layer-h-SiO_2 film. Two layers of hollow silica nanoparticles were precisely arranged in the film.

Figure 1c shows a cross-sectional TEM image of the antireflection film made from the AR-3 sample. The particles in this film were arranged in three to four stacked layers, with some overlap in the vertical direction in the case of the third and fourth layers. The particles were also relatively tightly packed without agglomeration. Because of this layer stacking, this film had a thickness of 165 nm, and so was thicker than those shown in Figure 1a,b. This specimen is the 3-layer-h-SiO_2 film. Figure 1d presents a cross-sectional TEM image of the antireflection film made using the AR-4 paint, which contained the dense silica particles with a particle diameter of approximately 60 nm. Although this film structure appears similar to that in Figure 1b, there were no cavities inside the particles. Hereafter, the antireflection coating made using the AR-4 paint is termed the 2-layer-d-SiO_2 film. Figure S2 shows the FE-SEM image of the 2-layer-d-SiO_2 film. Two layers of dense silica nanoparticles were precisely arranged in the film.

Figure 2 provides atomic force microscopy (AFM) images of the various antireflection films and demonstrates that, in each case, the nanoparticles were arranged with a relatively high degree of order. The R_a and R_{max} values were found to be 1.74 and 19.4 nm for the 1-layer-h-SiO_2 film, 2.80 and 26.1 nm for the 2-layer-h-SiO_2 film, 2.92 and 29.9 nm for the 3-layer-h-SiO_2 film, and 2.63 and 23.1 nm for the 2-layer-d-SiO_2 film, respectively. These values for a film composed only of PETA containing no particles were 0.17 and 1.82 nm, respectively. Thus, the R_a and R_{max} values for the films containing both hollow and dense nanoparticles were relatively high as a result of incorporating the nanoparticles. Even so, the surface roughness for each of these films was below that for a film made using only hollow silica nanoparticles without the PETA, for which the values were 3.52 and 39.2 nm. These results indicate that the gaps between the nanoparticles were filled

https://doi.org/10.1021/acsomega.1c00386
ACS Omega 2021, 6, 8570−8577

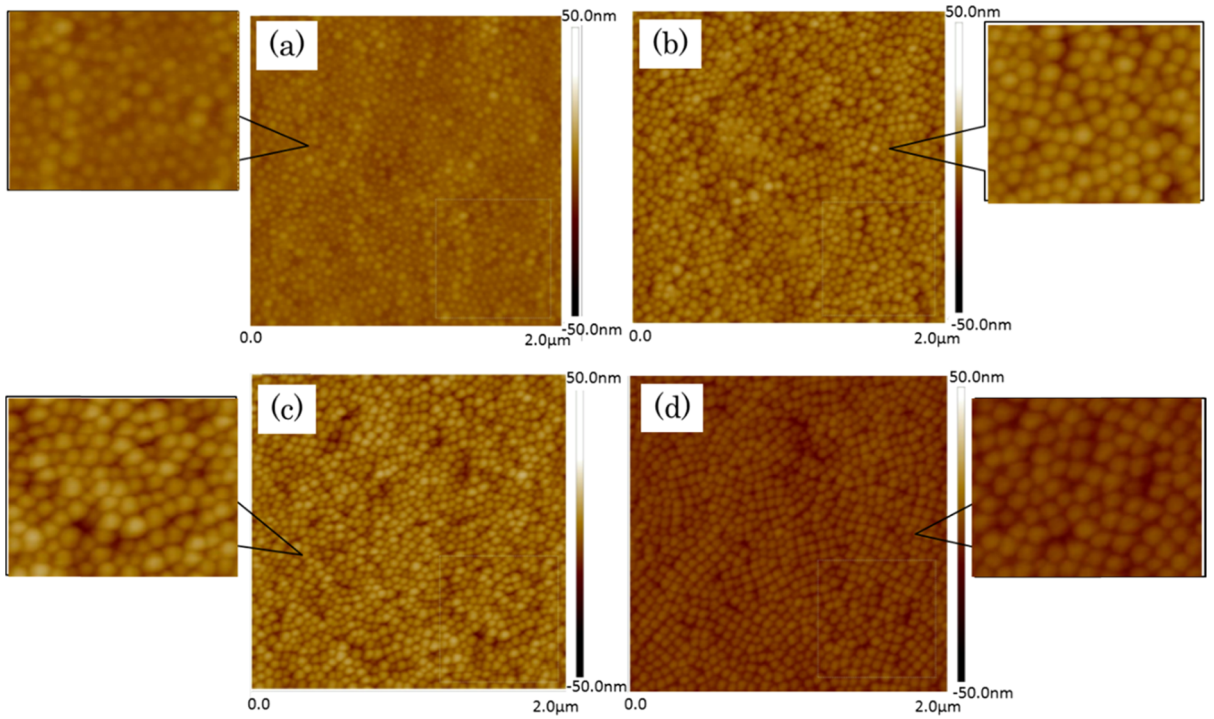

Figure 2. AFM images of (a) 1-layer-h-SiO_2, (b) 2-layer-h-SiO_2, (c) 3-layer-h-SiO_2, and (d) 2-layer-d-SiO_2 antireflection films.

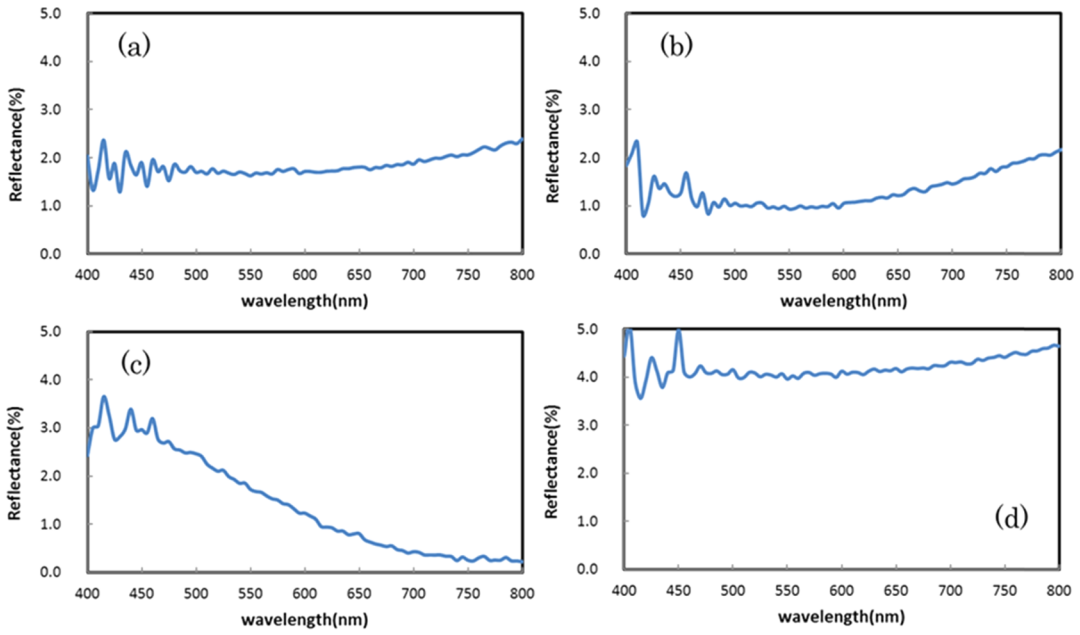

Figure 3. Reflectance plots for (a) 1-layer-h-SiO_2, (b) 2-layer-h-SiO_2, (c) 3-layer-h-SiO_2, and (d) 2-layer-d-SiO_2 antireflection films.

with resin and that the film surface was also covered with the polymer. The AFM images also confirm that the hollow silica nanoparticles were arranged in a relatively orderly manner without any appearance of aggregation.

Figure 3 shows the reflectance curves obtained for the antireflection films. The reflectance of the 1-layer-h-SiO_2 film changed with wavelength and the lowest reflectance of 1.62% appeared at 550 nm (Figure 3a). Figure 3b provides the data for the 2-layer-h-SiO_2 film and indicates a minimum reflectance of 0.92% at 550 nm wavelength. This value was significantly reduced compared to the reflectance of 4.33% for the bare TAC film. The curve for the 3-layer-h-SiO2 film in Figure 3c shows a reflectance minimum of 0.21% at 800 nm but a higher value of 1.72% at 550 nm, which is the center of the band to which the human eye is most sensitive. On this basis, it appears that the 2-layer-h-SiO_2 film exhibited the lowest reflectance at the most important wavelength among the various antireflection films. The wavelength at which the lowest wavelength of the 3-layer-h-SiO_2 film appeared was longer than those for the 1-layer-h-SiO_2 and 2-layer-h-SiO_2 films, which is ascribed to the differences in film thicknesses. Specifically, the 3-layer-h-SiO_2 sample (165 nm) was thicker than the 1-layer-h-SiO_2 (100 nm) and 2-layer-h-SiO_2 (100 nm) films, as shown in Figure 2. The relationship between the

https://doi.org/10.1021/acsomega.1c00386
ACS Omega 2021, 6, 8570−8577

thickness of an optical film, d, and the wavelength, λ, at which it presents its lowest reflectance can be summarized as

$$nd = \lambda/4 \quad (1)$$

where n is the refractive index of the film. Thus, λ becomes larger as the film becomes thicker. The low reflectance of the 2-layer-h-SiO_2 film is attributed not only to the orderly arrangement of the two nanoparticle layers but also to the use of hollow nanoparticles. As shown in Figure 3d, the reflectance at 550 nm for the 2-layer-d-SiO_2 film made of dense silica nanoparticles was much higher at 3.96%. This occurred because the lack of internal pores in the dense nanoparticles produced a higher refractive index.

Table 2 summarizes the reflectance values for the films at 550 nm wavelength along with the thicknesses and numbers of layers. All of the films made of hollow silica nanoparticles had a lower reflectance than the bare TAC substrate. However, even when the same hollow silica nanoparticles were used, the reflectance behavior differed greatly depending on the number of layers and the film thickness. Consequently, as noted above, the antireflection film with a thickness of about 100 nm and with hollow nanoparticles arranged in upper and lower stages (that is, two layers) showed the lowest reflectance. Figure 4 summarizes the experimental and simulated reflectance values for the films. The reflectance was calculated using the following eq 2 obtained from Fresnel's equation.

Table 2. Reflectance Values for Various Films at 550 nm

antireflection film	reflectance at 550 nm	number of particle layers	film thickness (nm)[a]
1-layer-h-SiO_2	1.62	1	100
2-layer-h-SiO_2	0.92	2	100
3-layer-h-SiO_2	1.72	3	165
2-layer-d-SiO_2	3.96	2	100
TAC substrate	4.33		

[a]Approximate values as determined by SEM.

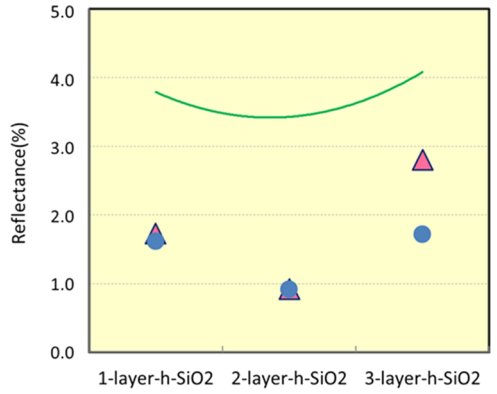

Figure 4. Reflectance of each antireflection film at a wavelength of 550 nm (●: measured value, Δ: plot when the refractive index of hollow particles is assumed to be n = 1.23, and solid line: when the film's refractive index is assumed to be n = 1.46 curve).

$$\text{reflectance: } R = \frac{r_1^2 + r_2^2 + 2r_1 \times r_2 \times \cos 2\delta}{1 + r_1^2 \times r_2^2 + 2r_1 \times r_2 \times \cos 2\delta} \quad (2)$$

where r_1 is the reflection of the AR film surface represented by eqn 3, r_2 is the reflection from the interface between the AR film and the TAC substrate represented by eq 4, and δ is the phase difference represented by eq 5

$$r_1 = (n_0 - n_1)/(n_0 + n_1) \quad (3)$$

$$r_2 = (n_1 - n_s)/(n_1 + n_s) \quad (4)$$

$$\delta = (2\pi/\lambda) \times n_1 \times d \quad (5)$$

where n_0 indicates the refractive index of air (n_0 = 1), n_1 is the refractive index of the AR film, which was calculated from the following eq 6, and n_s is the refractive index of the TAC substrate, which was set to 1.51. The wavelength λ was set to 550 nm, and d was the film thickness of the AR film, and the values in Table 2 were used.

$$n_1 = n_p \times V_p + n_r \times V_r \quad (6)$$

where the refractive index n_r of the cured resin portion was set to 1.51, and an arbitrary value was input to n_p of the refractive index of the particles. V_p is the volume ratio occupied by the particles in the AR film and V_r is the volume ratio occupied by the resin part in the AR film. These were obtained by image analysis of the simplified schematic cross-sectional model (Supporting Information Figure S3) from the TEM image in Figure 1. In making these models, it was assumed that the TEM images showed both foreground and background nanoparticles, and only the foreground nanoparticles were incorporated to avoid duplication. The simulation values obtained with an assumed refractive index of 1.23 for the hollow nanoparticles gave the best fit to the experimental data. From the calculation, the refractive index (1.23) was determined. Figure 4 also shows the simulated values generated using a refractive index of 1.46, which corresponds to that of pure silica. These values are obviously much larger than those for the actual films. These results confirm that a low reflective index for the film of 1.35 was achieved on the basis of a hybrid material consisting of an inorganic silica component with the gaps between nanoparticles filled by the UV-curable resin. Table 3 summarizes the total light transmittance (Tt) and film haze (Hz) of each antireflection film and show that the film haze was between 0.22 and 0.49% for all films, meaning that these values were equal to or lower than the value of 0.31% for the TAC substrate. This result suggests that agglomeration of the hollow silica nanoparticles did not occur, which is often a concern with these materials. Aggregation to form larger particles is undesirable because it increases light scattering due to voids and unevenness of the film surface. These internal and external scattering effects cause the film to appear whiter while also increasing the film haze such that optical transparency and image quality are reduced. The haze value for each film fabricated in this study was sufficient to maintain or improve the transparency of the substrate. That is, some specimens showed decreased haze compared with the TAC film.

Table 3. Total Light Transmittance and Film Haze Values for Each Antireflection Film

antireflection film	total light transmittance (%)	film haze (%)
1-layer-h-SiO_2	93.8	0.33
2-layer-h-SiO_2	95.2	0.22
3-layer-h-SiO_2	94.3	0.49
2-layer-d-SiO_2	92.8	0.22

https://doi.org/10.1021/acsomega.1c00386
ACS Omega 2021, 6, 8570−8577

Figure 5 shows the total light transmittance for each antireflection film. The 2-layer-h-SiO_2 film, which showed the lowest reflectance, had the highest transmittance value of 95.2%. This value exceeded that of the TAC substrate (92.6%). Figure 5 also shows that all of the antireflection films exhibited a higher total light transmittance than the TAC substrate. The 3-layer-h-SiO_2 film had the highest transmittance near 800 nm wavelength although this value dropped to approximately 94% near 550 nm. The 2-layer-h-SiO_2 film showed the highest total light transmittance near 550 nm wavelength.

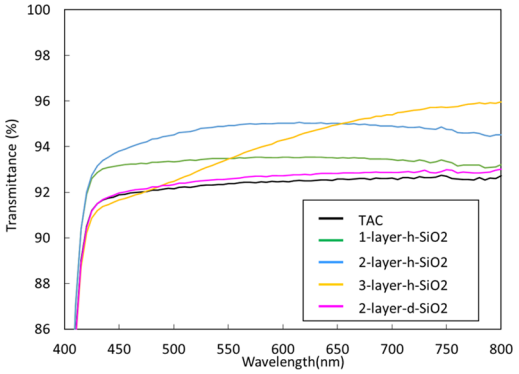

Figure 5. Total light transmittance for each antireflection film.

Optically transparent materials such as PET and TAC are suitable as base films for displays. However, because they are plastics and are applied as ultrathin films, they have low hardness and are easily damaged during handling and use. To solve this problem, a UV-curable hard coating serving as a protective layer and having a refractive index similar to that of the base film is generally applied at a thickness of several micrometers. In the present work, an antireflection film was formed on the TAC film in conjunction with a hard coating. Table 4 summarizes the pencil hardness of each antireflection film with a hard coat and demonstrates that each specimen had a pencil hardness in the range of H to 4H, all of which exceeded the value of <6B for the TAC substrate. Among these, the 2-layer-d-SiO_2 film showed the highest hardness, presumably because it incorporated the dense silica nanoparticles. In the case of the other three specimens, the pencil hardness decreased in the order 1-layer-h-SiO_2 film > the 2-layer-h-SiO_2 film > the 3-layer-h-SiO_2 film. This order agrees with the porosities seen in the cross-sectional TEM image in Figure 1. In addition, as seen in the film surface AFM images in Figure 2, the same order was present in the R_a and R_{max} values. These results suggest that the pencil hardness values were correlated with the film porosities and the surface roughnesses. Table 4 also indicates that the 2-layer-h-SiO_2 film on a hard-coated TAC substrate had a low reflectance of 1.37% and a high Tt value of 94.9% with a Hz value of 0.37%. In addition, the hardness of the TAC substrate, which is normally an issue, was greatly improved to a level that could allow practical applications.

Table 4. Pencil Hardness Values for Antireflection Films with Hard Coatings

antireflection film	pencil hardness	reflectance@550 nm (%)	total light transmittance (%)	film haze (%)
AR-1	4H	3.14	93.1	0.20
AR-2	H	1.37	94.9	0.37
AR-3	HB	3.25	92.6	0.24
AR-4	4H	3.52	93.0	0.33

CONCLUSIONS

A low-temperature film-forming process operating at 100 °C or lower was employed to apply thin films to plastic substrates. This process applied a UV-curable film as a simple one-layer coating using nanometer-sized hollow silica nanoparticles. The resulting structures formed transparent antireflection films without particle agglomeration or scattering, based on filling of the gaps between the nanoparticles. A specimen incorporating hollow silica nanoparticles having a diameter of approximately 60 nm and a silica shell thickness of 8 nm showed a reflectance of 0.92% at 550 nm wavelength, representing a reflectance reduction of nearly 80% relative to the bare TAC substrate. This film was approximately 100 nm thick and contained hollow silica nanoparticles arranged in two stages in the vertical direction. This specimen almost achieved the reflectance value of 1% required for general low-reflection performance. Cross-sectional TEM images and AFM analyses confirmed that the nanoparticles were arranged inside the UV cured film and that the film surface was sufficiently covered by the organic binder. Also, there were no voids due to particle gaps inside the film, and the haze value of the films was low and the material was highly transparent. This extremely inexpensive and simple coating system should be well suited to film formation over large areas using techniques such as the roll-to-roll method. This process could potentially be employed to prevent reflections on various electronic devices such as televisions, computer monitors, and smartphones.

EXPERIMENTAL SECTION

Materials. Both a hollow silica sol (Thrulya4320, JGC Catalyst and Chemicals Ltd., Kanagawa, Japan) and dense silica sol (ELCOM V-8805, mean diameter: 45 nm, JGC Catalyst and Chemicals Ltd., Kanagawa, Japan) were used in this work. Acetone (≥99.0%, Hayashi Pure Chemical Ind., Ltd., Osaka, Japan), isopropyl alcohol (IPA, ≥99.9%, Mitsui Chemicals Inc., Tokyo, Japan), propylene glycol monomethyl ether (PGM, ≥99.0%, Nippon Nyukazai Co., Ltd., Tokyo, Japan), and methyl isobutyl ketone (MIBK, Mitsubishi Chemical Corporation, Tokyo, Japan) were employed as solvents. Pentaerythritol triacrylate (PETA, Light acrylate PE-3A, Kyoeisha Chemical Co., Ltd., Osaka, Japan) was used as the UV-curable acrylate resin and hydroxy cyclohexylphenyl ketone (HCPK, ≥99.0%, Omnirad 184, IGM Resins B. V. Waalwijk, Netherlands) was used as the polymerization photoinitiator. Triacetyl cellulose (TAC) film specimens (thickness: 80 μm, Fuji film Corp.) were employed as transparent plastic substrates and were cleaned under a flow of air before use.

Preparation of UV-Curable Antireflection Coating Paints. Quantities of hollow silica sol (silica concentration 20.5 wt %), IPA, MIBK, PETA, and HCPK were mixed in amber bottles according to the blending ratios in Table 1, after which each mixture was vigorously stirred to produce three types of UV-curable antireflection coating paints (AR-1, AR-2, and AR-3). A coating paint (AR-4) instead made with the dense silica nanoparticles was also prepared according to the blending ratio in Table 1 as a reference. The hollow silica sol

https://doi.org/10.1021/acsomega.1c00386
ACS Omega 2021, 6, 8570−8577

easily aggregated with the organic resin. Therefore, hollow silica sol was mixed with IPA and MIBK solvents to dilute the silica sol concentration and then mixed with organic resin monomers to prevent agglomeration (Scheme 1). By adopting this scheme, a stable transparent film can be obtained while suppressing aggregation and whitening of the film that occur when the hollow silica sol and the organic resin monomer are directly mixed. Further, the mixing was carried out in an amber bottle and the initiator was mixed in the latter half so that an unnecessary photocuring reaction did not occur in advance.

Preparation of Antireflection Coating Films. The AR-1, AR-2, AR-3, and AR-4 paints were diluted, respectively, to 3.00, 2.90, 0.28, and 2.90 wt % with a 7/3 IPA/MIBK mixture. A quantity of 1 mL each diluted sample was dropped onto a 14 × 21 cm portion of a TAC substrate and applied with a #4 bar coater to give a wet film thickness of 9.1 μm, using a sweep rate of 80 mm/s. Note that a #6 bar coater was employed to process the AR-4 sample, giving a wet film thickness of 13.7 μm. The antireflection films were coated using an automated device (Auto Film Applicator, model PI-1210, TESTER Sangyo Co., Ltd., Japan). After coating, each film was allowed to dry for 2 min in a drying box at 80 °C (VTN-111, ISUZU Seisakusyo Co., Ltd., Japan), after which the film was transferred into a sealed container having a quartz lid that had been purged with nitrogen and had an oxygen concentration of less than 100 ppm. Each coated and dried TAC film was exposed to UV light using an electrodeless lamp with a hydrogen bulb (Heraeus, Inc.) at a power level of 400 mJ/cm^2 while remaining in the container so as to cure the polymer (Scheme 2).

Scheme 2. Preparation of Antireflection Coating

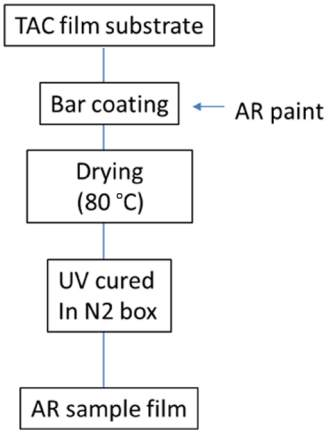

Preparation of UV-Curable Hard Coating paint. PETA (4.00 g), PGM (4.80 g), acetone (1.00 g), and HCPK (0.20 g) were mixed in a shading bottle and stirred for 1 min, which was used as a hard coating paint.

Preparation of a Hard Coating Film. Hard coating paint (1 mL) was dropped on a TAC film (cut to 14 cm × 21 cm) and applied with a bar coater #10 at a sweep rate 80 mm/s. The coated film was dried for 2 min at 80 °C in a drying box. We obtained hard coating film after the film was 300 mJ/cm^2 UV cured using a H bulb manufactured by Heraeus, Inc.

Preparation of an Antireflection Coating Film with Hard Coating. We obtained an antireflection coating film with a hard coat layer by coating, drying, and UV curing, as shown below, onto a TAC film with hard coating using AR-1, AR-2, AR-3, and AR-4 samples. AR-1, AR-2, AR-3, and AR-4 samples were diluted, respectively, to 2.40, 2.25, 2.60, and 2.70 wt % by IPA/MIBK = 7/3 mixed solvent. One milliiter of each diluted sample was dropped onto the TAC film with a hard coat set in a coating device (PI-1210) and applied with a bar coater #4 at a sweep rate of 80 mm/s. After coating, the film was dried for 2 min at 80 °C in a drying box, and then the film was put into a N_2 purge box with N_2 gas replacement below 100 ppm O_2 concentration. The film was UV cured at 400 mJ/cm^2 while still in the N_2 purge box by an electrodeless lamp bulb. We finally obtained an antireflection coating film with hard coating.

Characterization. Cross-sectional observations of the films were performed using field-emission transmission electron microscopy (FE-TEM, HF-2200, Hitachi High-Tech Corp.). The samples for cross-sectional observations were cut to a thickness of less than 100 nm with an ultramicrotome (EM UC7, Leica Microsystems Inc.) and then placed on a copper microgrid. The average surface roughness and maximum in-plane height difference values (R_a and R_{max}) of the films were determined using atomic force microscopy (AFM, Dimension 3100, Bruker) over areas of 2.0 × 2.0 μm. The reflectance of each film was measured with a spectroscopic film thickness meter (FE-3000, Otsuka Electronics Co., Ltd.). Prior to each analysis, the back surface of the TAC substrate was coated with a black marker to suppress back surface reflection. The total light transmittance and the film haze were measured by a haze meter (NDH-5000, Nippon Denshoku Industries Co., Ltd.) and a UV−visible spectrophotometer (V-760, JASCO Corp.). Pencil hardness was measured with ISO15184, JIS K-5600-5-4.

■ ASSOCIATED CONTENT

Supporting Information

The Supporting Information is available free of charge at https://pubs.acs.org/doi/10.1021/acsomega.1c00386.

FE-SEM image of the surface of 2-layer-h-SiO_2 (Section S1), the FE-SEM image of the surface of 2-layer-d-SiO_2 (Section S2), model structures obtained from cross-sectional TEM images for 1-layer-h-SiO_2, 2-layer-h-SiO_2, and 3-layer-h-SiO_2 antireflection films (Section S3), and reflectance plots for 2-layer-h-SiO_2 antireflection films with hard coating (Section S4) (PDF)

■ AUTHOR INFORMATION

Corresponding Authors

Ryo Muraguchi − *Institute of Industrial Nanomaterials, Kumamoto University, Kumamoto 860-8555, Japan; Fine Chemicals Research Center, JGC Catalysts and Chemicals Ltd., Kitakyushu 808-0027, Japan*; Email: muraguchi.ryo@jgccc.com

Shintaro Ida − *Institute of Industrial Nanomaterials, Kumamoto University, Kumamoto 860-8555, Japan*; orcid.org/0000-0002-0032-1897; Email: ida-s@kumamoto-u.ac.jp

Authors

Wataru Futagami − *Fine Chemicals Research Center, JGC Catalysts and Chemicals Ltd., Kitakyushu 808-0027, Japan*

Yuko Hakoshima − *Fine Chemicals Research Center, JGC Catalysts and Chemicals Ltd., Kitakyushu 808-0027, Japan*

Keisuke Awaya − *Institute of Industrial Nanomaterials, Kumamoto University, Kumamoto 860-8555, Japan*

https://doi.org/10.1021/acsomega.1c00386
ACS Omega 2021, 6, 8570−8577

Complete contact information is available at:
https://pubs.acs.org/10.1021/acsomega.1c00386

Notes

The authors declare no competing financial interest.

■ ACKNOWLEDGMENTS

This work was supported by the JGC Catalysts and Chemicals Ltd. and the Institute of Industrial Nanomaterials at Kumamoto University.

■ ABBREVIATIONS

TAC, triacetyl cellulose; IPA, isopropyl alcohol; PGM, propylene glycol monomethyl ether; MIBK, methyl isobutyl ketone; PETA, pentaerythritol triacrylate; HCPK, hydroxy cyclohexylphenyl ketone

■ REFERENCES

(1) Bao, Y.; Shi, C.; Wang, T.; Li, X.; Ma, J. Recent progress in hollow silica:template synthesis;morphologies and applications. *Microporous Mesoporous Mater.* **2016**, *227*, 121−136.
(2) Varol, H. S.; Alvarez-Bermudez, O.; Dolcet, P.; Kuerbanjiang, B.; Gross, S.; Landfester, K.; Munoz-Espi, R. Crystallization at nano-droolet interfaces in emulsion systems:a soft-template strategy for preparing porous and hollow nanoparticles. *Langmuir* **2016**, *49*, 13116−13123.
(3) Li, Y.; Kruk, M. Single-micelle-templated synthesis of hollow silica nanospheres with tunable pore structures. *RSC Adv.* **2015**, *85*, 69780−69877.
(4) Liu, X.; Jiao, Z.; Song, T.; Wu, M.; Zhang, H. Surfactant-assisted selective etching strategy for generation of rattle-like mesoporous silica nanoparticles. *J. Colloid Interface Sci.* **2017**, *490*, 497−504.
(5) Li, J.; Chen, L. X.; Li, X.; Zhang, C. C.; Zeng, F. L. Hollow organosilica nanospheres prepared through surface hydrophobic layer protected selective etching. *Appl. Surf. Sci.* **2015**, *340*, 126−131.
(6) Zhang, T.; Ge, J.; Hu, Y.; Zhang, Q.; Aloni, S.; Yin, Y. Formation of Hollow Silica Colloids through a Spontaneous Dissolution-Regrowth Process. *Angew. Chem., Int. Ed.* **2008**, *47*, 5806−5811.
(7) Zhang, Q.; Zhang, T.; Ge, J.; Yin, Y. Permeable silica shell through surface-protected etching. *Nano Lett.* **2008**, *8*, 2867−2871.
(8) Yu, Q.; Wang, P.; Hu, S.; Hui, J.; Zhuang, J.; Wang, X. Hydrothermal Synthesis of Hollow Silica Spheres under Acidic Conditions. *Langmuir* **2011**, *27*, 7185−7191.
(9) Yildirim, A.; Bayindir, M. A porosity difference based selective dissolution strategy to prepare shape-tailored hollow mesoporous silica nanoparticles. *J. Mater. Chem. A* **2015**, *3*, 3839−3846.
(10) Nomoev, A. V. Synthesis and properties of hollow silica nanoparticles. *Tech. Phys. Lett.* **2012**, *38*, 466−469.
(11) Perales, F.; Herrero, J. M.; Jaque, D.; De las Heras, C. Improvement of MgF2 thin coating films for laser applications. *Opt. Mater.* **2007**, *29*, 783−787.
(12) Bruynooghe, S.; Tonova, D.; Sundermann, M.; Koch, T.; Shulz, U. Antireflection coatings combining interference multilayers and a nanoporous MgF_2 top layer prepared by glancing angle deposition. *Surf. Coat. Technol.* **2015**, *267*, 40−44.
(13) Xi, J.; Schubert, M.; Kim, J.; Schubert, E.; Chen, M.; Lin, S.; Liu, W.; Smart, J. Optical thin-film materials with low refractive index for broadband elimination of Fresnel reflection. *Nat. Photonics* **2017**, *1*, 176−179.
(14) Zhang, J.; Lan, P.; Li, J.; Xu, H.; Wang, Q.; Zheng, L.; Lu, Y.; Dai, N.; Song, W. Sol-gel derived near-UV and visible antireflection coatings from hybridized hollow nanospheres. *J. Sol-Gel Sci. Technol.* **2014**, *71*, 267−275.
(15) Zhang, X.; Lu, Q.; Cheng, Y.; Liu, L.; Shan, Y.; Zhang, Q.; Li, D. Moth-eye-like antireflection coatings based on close-packed solid/hollow silica nanospheres. *J. Sol-Gel Sci. Technol.* **2019**, *90*, 330−338.
(16) Zhang, J.; Ai, L.; Lin, S.; Lan, P.; Lu, Y.; Dai, N.; Tan, R.; Fan, B.; Song, W. Preparation of humidity; abrasion; and dust resistant antireflection coatings for photovoltaic modules via dual precursor modification and hybridization of hollow silica nanospheres. *Sol. Energy Mater. Sol. Cells* **2019**, *192*, 188−196.
(17) Guo, Z.; Zhao, H.; Zhao, W.; Wang, T.; Kong, D.; Chen, T.; Zhang, X. High-Quality Hollow Closed-Pore Silica Antireflection Coatings Based on Styrene-Acrylate Emulsion @ Organic-Inorganic Silica Precursor. *ACS Appl. Mater. Interfaces* **2016**, *8*, 11796−11805.
(18) Gao, T.; Jelle, B. P.; Gustavsen, A. Antireflection properties of monodisperse hollow silica nanospheres. *Appl. Phys. A* **2013**, *110*, 65−70.
(19) Tao, C.; Zou, X.; Du, K.; Zhang, L.; Yan, H.; Yuan, X. Ultralow-refractive-index optical thin films built from shape-tunable hollow silica nanomaterials. *Opt. Lett.* **2018**, *43*, 1802−1805.
(20) Suthabanditpong, W.; Tani, M.; Takai, C.; Buntem, R.; Shirai, T. Facile fabrication of light diffuser films based on hollow silica nanoparticles as fillers. *Adv. Powder Technol.* **2016**, *27*, 454−460.
(21) Malitson, I. H. Interspecimen Comparison of the Refractive Index of Fused Silica. *J. Opt. Soc. Am.* **1965**, *55*, 1205−1209.
(22) Zhang, X. T.; Sato, O.; Taguchi, M.; Einaga, Y.; Murakami, T.; Fujishima, A. Self-Cleaning Particle Coating with Antireflection Properties. *Chem. Mater.* **2005**, *17*, 696−700.
(23) Hattori, H. Anti-Reflection Surface with Particle Coating Deposited by Electrostatic Attraction. *Adv. Mater.* **2001**, *13*, 51−54.
(24) Zou, X.; Tao, C.; Yang, K.; Yang, F.; Lv, H.; Yan, L.; Yan, H.; Li, Y.; Xie, Y.; Yuan, X.; Zhang, L. Rational design and fabrication of highly transparent; flexible; and thermally stable superhydrophobic coatings from raspberry-like hollow silica nanoparticles. *Appl. Surf. Sci.* **2018**, *440*, 700−711.
(25) Tao, C.; Yan, H.; Yuan, X.; Yao, C.; Yin, Q.; Zhu, J.; Ni, W.; Yan, L.; Zhang, L. Synthesis of shape-controlled hollow silica nanostructures with a simple soft-templating method and their application as superhydrophobic antireflective coatings with ultralow refractive indices. *Colloids Surf., A* **2016**, *501*, 17−23.
(26) Zhang, X.; Lan, P.; Lu, Y.; Li, J.; Xu, H.; Zhang, J.; Lee, Y. P.; Rhee, J. Y.; Choy, K. L.; Song, W. Multifunctional Antireflection Coatings Based on Novel Hollow Silica-Silica Nanocomposites. *ACS Appl. Mater. Interfaces.* **2014**, *6*, 1415−1423.
(27) Tao, C.; Yan, H.; Yuan, X.; Yin, Q.; Zhu, J.; Ni, W.; Yan, L.; Zhang, L. Sol-gel based antireflective coatings with superhydrophobicity and exceptionally low refractive indices built from trimethylsilanzed hollow silica nanoparticles. *Colloids Surf., A* **2016**, *509*, 307−313.
(28) Jia, G.; Ji, Z.; Wang, H.; Chen, R. Preparation and properties of five-layer graded-refractive-index antireflection coating nanostructured by solid and hollow silica particles. *Thin Solid Films* **2017**, *642*, 174−181.
(29) Ye, L.; Li, L.; Wang, X.; Zhang, Y.; Yan, L. Template-free synthesis of uniform hollow silica nanoparticles for controllable antireflection coatings. *Ceram. Int.* **2020**, *46*, 7453−7458.
(30) Du, Y.; Luna, L. E.; Tan, W. S.; Rubner, M. F.; Cohen, R. E. Hollow silica nanoparticles in UV−visible antireflection coatings for poly(methyl methacrylate) substrates. *ACS Nano* **2010**, *4*, 4308−4316.